Urban Heat Island Characterization with Airborne Thermal Infrared Hyperspectral Imaging

The higher concentration of man-made objects like asphalt pavement and concrete structures within urban areas lead to the formation of subareas known as urban heat islands (UHI), where the ambient temperature is significantly higher. Having a good understanding of this problem is critical for better urban development. Thermal infrared (TIR, 8-12 µm) remote sensing is often used to localize UHI. However, surface temperature measurement using conventional broadband TIR sensors cannot account for the spectral emissivity properties of the materials leading to erroneous surface temperature estimates. In this work, airborne TIR hyperspectral imaging (HSI) was carried out on urban areas at high spectral resolution. The thermodynamic temperature maps obtained after temperature-emissivity separation (TES) display sharper thermal contrast associated with UHI, making their identification easier. A chemical map of quartz (SiO_2), a material used in the fabrication of many buildings and roads, highlights the close association between UHI and man-made objects.

Introduction

Temperature measurement plays a decisive role in the characterization of urban heat islands (UHI). An UHI is an area that is characterized by an average temperature significantly higher than its surroundings as a result of a higher concentration of man-made objects like asphalt pavement and concrete structures (see Figure 1). The later absorbs solar radiation and reemits the energy as thermal infrared radiation. Consequently, the average temperature measured in an UHI is higher than what would be measured in less populated areas, such as rural environments, on the same day [1].

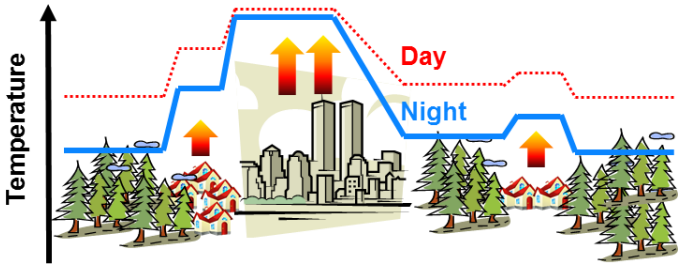

Figure 1 Illustration of the urban heat island effect.

A traditional way of characterizing temperature gradients on vast areas is thermal infrared (TIR) remote sensing (8 to 12 µm) [2]. Both broadband and multispectral TIR imaging provide radiometric temperature values, which can be assumed as representative of the thermodynamic surface temperature. However, the temperature values obtained from remote sensing measurements contain a portion of both infrared self-emission and reflection. Since the somewhat "cold" sky radiance represents the main irradiance source in outdoor measurements, low-emissivity, i.e. highly reflective, surfaces appears unreasonably cold. The challenges associated with remote temperature measurements are well-represented in Figure 2 where various surfaces such as vegetation, soils, wood, aluminum, concrete and asphalt pavement all appear to be at very different temperatures despite being in similar environmental conditions.

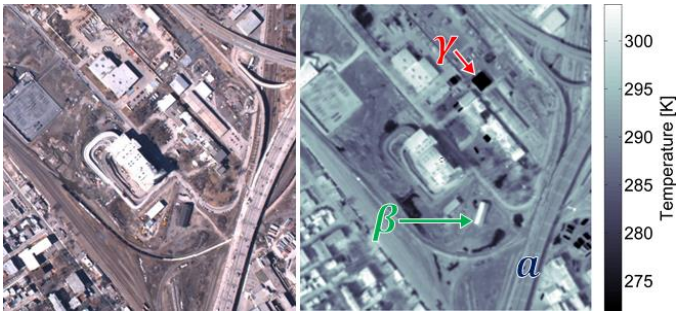

Figure 2 Airborne visible image (left) and broadband infrared temperature map (right) of an industrial area. Selected locations are labeled for further explanations.

The chemical nature of the investigated material greatly affect the temperature readings when using a broadband TIR sensor. As an example, some objects in Figure 2 display temperatures well above (pixels α and β) and below (pixel γ) water's freezing point, which is quite unlikely considering their vicinity. Other surfaces like the road pavement display temperature values in between these two "extreme" cases. All these surfaces are well-known to have very different emissivity properties, i.e. they are more or less reflective in the TIR spectral range. In order to illustrate this point, the high resolution infrared spectra associated with these locations are shown on a brightness temperature scale in Figure 3.

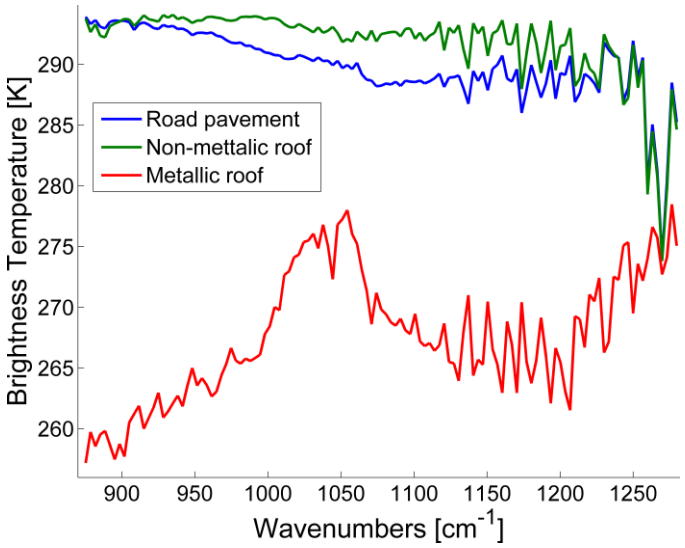

Figure 3 Airborne TIR spectra of selected pixels labeled in Figure 2. The blue curve is associated with road pavement. The green and red curves are associated with a non-metallic and metallic roof respectively.

On such a scale, one can see that the "temperature" appears to vary as a function of wavenumber (or wavelength) as a result of infrared absorption/self-emission from the targets in the sensor's line of sight. It can be seen that all three display very different spectral features. Metallic surfaces are typically known for being low-emissivity materials. For this reason, the spectral features seen in the red curve of Figure 3 (pixel γ of Figure 2) share a lot of similarities with the sky's spectral radiance. This kind of observation is somewhat expected as the roof faces the sky from an airborne perspective.

The non-metallic roof and the road pavement depict totally different behaviors. The spectrum associated with the black roof (green curve) suggests that this surface has a relatively high emissivity since most of the sharp spectral features in the 1100-1275 cm^{-1} spectral range correspond to absorption bands from atmospheric water vapor. In addition, the reflective nature of the material is wavenumber (or wavelength) dependent as a result of its infrared absorption/emission band, which is unique to each molecule. Therefore, one must estimate both the surface's spectral emissivity and self-emission contribution to the measurement in order to estimate accurately the surface's thermodynamic temperature. This procedure is known as temperature-emissivity separation (TES) and is described elsewhere in more detail [3, 4].

Airborne thermal infrared hyperspectral mapping was carried out over urban areas containing a great diversity of natural and man-made objects. The TES algorithm was applied to the data which gave two results: a thermodynamic temperature map and a spectral emissivity datacube.

The temperature contrast associated with UHI was found to be sharper on the thermodynamic temperature map obtained after TES than on the radiometric temperature map, making their identification easier. A chemical map of quartz (SiO_2), a material used in the fabrication of many building and road construction, was derived from the spectral emissivity datacube. The results highlight the close association between UHI and man-made objects.

Experimental Information

The Telops Hyper-Cam Airborne Platform

All measurements were carried out using the Telops Hyper-Cam airborne platform. The Hyper-Cam-LW (longwave) is a lightweight and compact hyperspectral imaging instrument that uses Fourier Transfer Infrared (FTIR) technology. The Telops Hyper-Cam features a focal

plane array (FPA) detector containing 320 × 256 pixels over a basic 6.4° × 5.1° field of view (FOV). For the experiment, the FOV was extended to 25.6° × 20.4° using a de-magnifying 0.25 × telescope. In its airborne configuration, the spectral resolution is user-selectable up to 1 cm^{-1} over the 7.7 µm (1300 cm^{-1}) to 11.8 µm (855 cm^{-1}) spectral range. The Telops Hyper-Cam airborne platform is equipped with a global positioning system (GPS) and an inertial motion unit (IMU) for geo-referencing and tracking of the aircraft movements in flight. An image-motion compensation (IMC) mirror uses the GPS/IMU data to compensate efficiently for the aircraft movements during data acquisition since acquiring a full datacube typically lasts about one second. The data includes all the relevant information for orthorectification and stitching. Visible images are simultaneously recorded along with the infrared datacubes using a boresight CCD camera on the airborne platform.

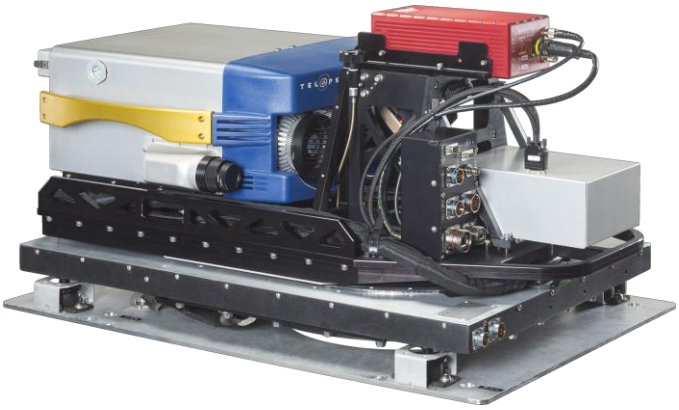

Figure 4 The Telops Hyper-Cam airborne platform.

Flight Conditions

The first flight was carried out in the southeastern portion (GPS position: 46.827279, -71.219555) of Quebec City (Canada) in April 2013 around 3 PM at an altitude of 2150 meters and a speed of 110 knots, leading to a ground pixel size of 9 m^2/pixel. A spectral resolution of 4 cm^{-1} was used, which gives a total of 125 spectral bands over the whole range covered by the FPA detector. Ambient temperature and relative humidity at ground level were 11 °C and 30 % respectively.

Data Processing

Radiometric temperature maps were obtained by computing the mean values of each pixel put on a brightness temperature scale. Temperature emissivity separation (TES) was carried out by solving Eq. 1, where L is the radiance measured at the sensor level, $\varepsilon_{\bar{\nu}}$ the target spectral emissivity, Dw the effective downwelling radiance on the target, $L_{surface}$ the target's self-emission (which is function of its thermodynamic temperature as described by the Planck equation), τ_{atm} is the atmospheric transmittance, and L_{atm} the radiance associated with TIR self-emission of all atmospheric components.

Equation 1

$$L = \left[L_{surface}\varepsilon_{\bar{\nu}} + Dw(1-\varepsilon_{\bar{\nu}})\right]\tau_{atm} + L_{atm}(1-\tau_{atm})$$

A smoothing criterion, similar to the one described in the work of Borel [4] was used to minimize both atmospheric and downwelling radiance contributions. Radiometric temperature maps were obtained by calculating, for each pixel, the mean brightness temperature value over the detector's whole spectral range.

Quartz chemical imaging was carried out by estimating the relative contributions (coefficients $A, B \ldots$) of the different components ($\varepsilon_{\bar{\nu}_n}$) within the overall spectral emissivity ($\varepsilon_{\bar{\nu}_{tot}}$), as shown in Eq. 2.

Equation 2

$$\varepsilon_{\bar{\nu}_{tot}} = A\varepsilon_{\bar{\nu}_1} + B\varepsilon_{\bar{\nu}_2} + C\varepsilon_{\bar{\nu}_3} + \mathrm{D}\varepsilon_{\bar{\nu}_n}$$

Results and Discussion

From an airborne TIR perspective, thermal contrasts mostly originate from an energy balance between a self-emission component from a surface under ambient conditions and a reflection component mostly associated with sky radiance, which is much lower in amplitude. Sky radiance is a complex mixture of infrared signals from cold gases (like water vapor, nitrous oxide, ozone,

methane and carbon dioxide) at various temperature and pressure conditions. It is well-known that the spectral features associated with gases are much narrower than the ones of solid materials. Therefore, collecting infrared hyperspectral data at a high spectral resolution represents a real advantage in this case as it eases the TES procedure.

Thermodynamic Temperature Map

A visible image of the surveyed area is presented in Figure 5. The scene contains a great variety of environments such as a parks (vegetation), residential areas (houses), highway roads and industrial areas (factory plants, fuel tanks, ship …). The corresponding thermodynamic temperature map, equivalent to what would be obtained with a broadband TIR sensor, is also presented. Sufficient thermal contrasts are present in the scene for clear identification of these very different environments. The corresponding thermodynamic temperature map, obtained after TES, is also presented on the same temperature scale. At first sight, the UHI resulting from the residential area is more obvious in the thermodynamic temperature map since sharper contrasts are obtained. As expected, the industrial areas are also warmer than the harbor and the parks. This contrast enhancement results from accounting for both atmospheric absorption and reflections from a "cold" sky. In addition, no "unrealistic" ground temperature values can be found in the thermodynamic temperature map.

As expected, most temperature values are higher than their corresponding brightness temperature values since the reflection of a cold irradiance source, i.e. the sky, and the atmospheric contribution have been accounted for. The atmospheric absorption creates a systematic temperature offset in the radiometric temperature values. Since the TES procedure accounts for such effect, it is expected that the thermodynamic temperature values are higher than their corresponding radiometric temperature values. As expected, vegetation and water areas are cooler than the residential and industrial areas.

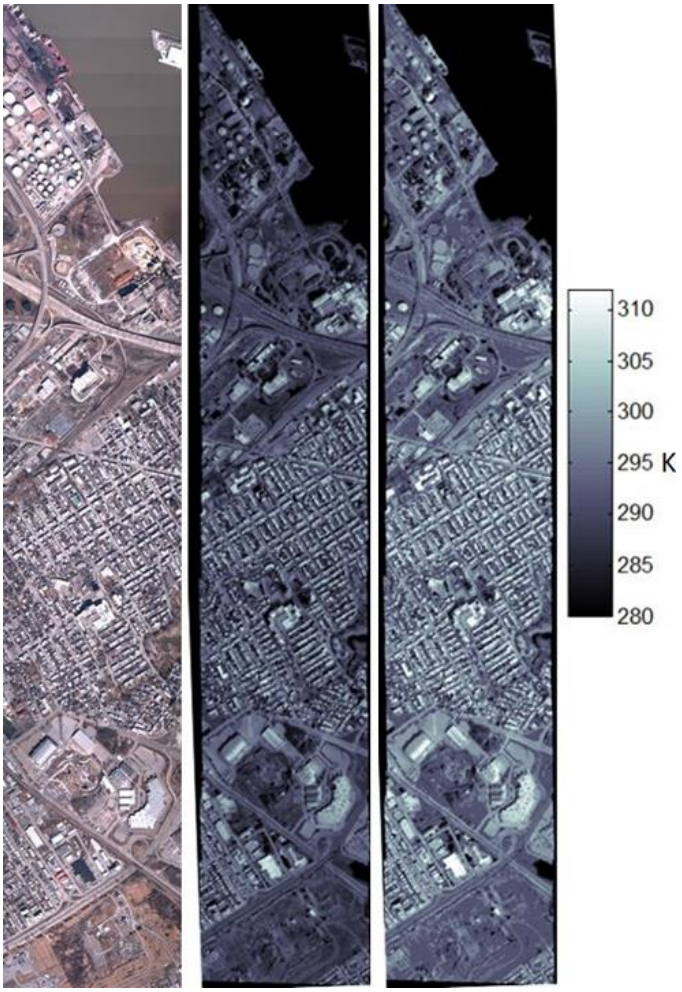

Figure 5 Visible image (left), radiometric temperature map (center) and thermodynamic temperature map (right) of urban areas.

Quartz Chemical Mapping

The spectral emissivity datacubes associated with the whole survey area contain the information about the mineral composition of the ground surface. However, since pure substances are not likely to be found on the order of the ground pixel size, spectral unmixing must be carried out on the data using basic spectral emissivity components. The resulting chemical map for quartz is shown in Figure 6. Quartz is often encountered in soils and sand, and used in the production of many materials such as concrete and asphalt. Therefore, it is not surprising to detect quartz in urban areas.

A larger representation of an industrial area is also shown in Figure 6 where fuel tank installations are surrounded

by concrete slabs. Comparison with the visible image suggests that the quartz chemical imaging results are in good agreement with the presence of concrete.

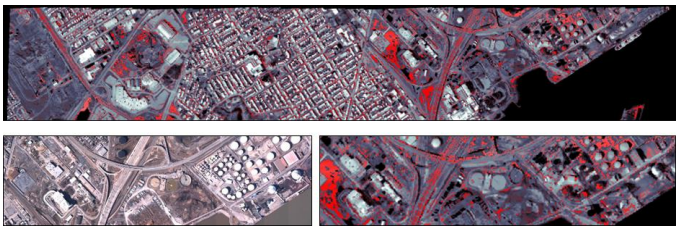

Figure 6 Quartz chemical map (red) obtained from linear unmixing of the spectral emissivity data. The results are displayed over the radiometric temperature map (grey scale) for clarity purposes. A larger representation of an industrial area is shown (bottom right) as well as its associated visible image (bottom left).

Quartz is not the only mineral that can be detected by TIR nor the only one present in urban areas. However, since it is among the most abundant mineral used in the fabrication of urban structures, its geographical distribution can be used to emphasize the presence of man-made objects within a surveyed area. Comparison of thermal (Figure 5) and chemical (Figure 6) information suggests a close relationship between man-made material and the presence of UHI.

Conclusion

Airborne TIR hyperspectral data recorded at a high spectral resolution allows efficient compensation of atmospheric and sky reflection contributions in the measured radiance. The thermodynamic temperatures estimated from the TES algorithm emphasizes the temperature contrasts resulting from the higher concentration of high-emissivity materials found in urban areas. The chemical map of quartz emphasizes the presence of man-made objects within the surveyed area. Combination of thermal and chemical information provides a better understanding of the relationship between man-made materials and UHI. The results show that airborne TIR hyperspectral imaging (HSI) provides a valuable approach for the characterization of urban heat islands.

References

[1] A.J. Arnfield, "Two Decades of Urban Climate Research: A Review of Turbulence, Exchanges of Energy and Water, and the Urban Heat Island," *Int. J. Climatol.*, 23, 1-26 (2003).

[2] C.P. Lo, D.A. Quattrochi and J.C. Luvall, "Application of High-Resolution Thermal Infrared Remote Sensing and GIS to Assess the Urban Heat Island Effect,'' *Int. J. Remote Sensing*, 18, 287-304 (1997).

[3] A.R. Gillespie, *et al.*, *Temperature/Emissivity Separation Algorithm Theoretical Basis Document*, Version 2.4, NASA, 64 p. (1999).

[4] Airborne Thermal Infrared Hyperspectral Imaging for Mineral Mapping, Application Note, Telops (2015).

[5] C.C. Borel, ARTEMISS – an Algorithm to Retrieve Temperature and Emissivity from Hyper-Spectral Thermal Image Data, 28th Annual GOMACTech Conference, Hyperspectral Imaging Session (2003).

Telops

100-2600 St-Jean-Baptiste Ave
Quebec (QC) Canada G2E 6J5
Tel: +1-418-864-7808 info@telops.com
Fax: +1-418-864-7843 www.telops.com